Unveiling the mysterious hydrocarbon – Clar's goblet

Tianyu Jiao[1], Cong-Hui Wu[2], Yu-Shuang Zhang[2], Xiaohe Miao[3], Shaofei Wu[1], Shang-Da Jiang[2]*, and Jishan Wu[1]*

[1]Department of Chemistry, National University of Singapore, 3 Science Drive 3, Singapore 117543

[2]Spin-X Institute, School of Chemistry and Chemical Engineering, State Key Laboratory of Luminescent Materials and Devices, Guangdong-Hong Kong-Macao Joint Laboratory of Optoelectronic and Magnetic Functional Materials, South China University of Technology, Guangzhou 511442, China

[3]Instrumentation and Service Center for Molecular Sciences, Westlake University, Hangzhou 310030, Zhejiang, China

*e-mail: chmwuj@nus.edu.sg (J. W.) and jiangsd@scut.edu.cn (S.-D. J.)

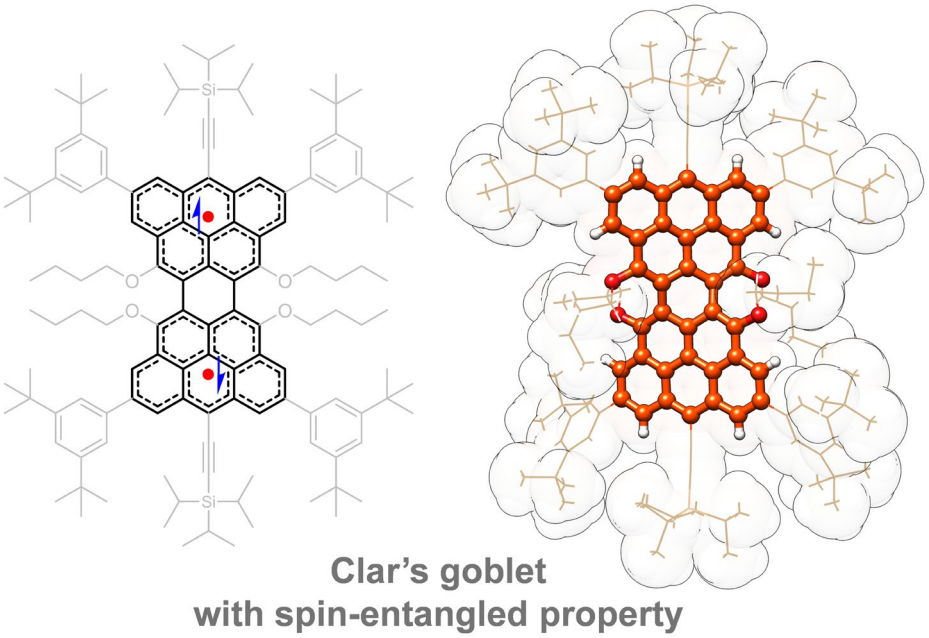

In the classic view, spin pairing occurs between two electrons in a chemical bond where the bonding interaction compensates for the penalty of electrostatic repulsion. It is a mystery whether spin pairing can occur between two non-bonded electrons within a molecular entity. Unveiling this elusive spin entanglement (i.e., pairing between two spatially segregated spins) at the molecular scale, is a long-standing challenge. Clar's goblet proposed by Erich Clar in 1972, provides an ideal model to verify this unusual property. Here, we report the solution-phase synthesis of Clar's goblet and experimental elucidation of its spin properties. Magnetic studies reveal that the two spins are spatially segregated with an average distance of 8.7 Å, and antiferromagnetically coupled in the ground state with an $\Delta E_{S\text{-}T}$ of –0.29 kcal/mol. Our results provide direct evidence of spin entanglement in the Clar's goblet and may inspire the design of correlated molecular spins for quantum information technologies.

https://doi.org/10.26434/chemrxiv-2024-ks6xm **ORCID:** https://orcid.org/0000-0002-8231-0437 Content not peer-reviewed by ChemRxiv. **License:** CC BY 4.0

The story of Clar's goblet dates back to 1972, when Erich Clar envisioned this mysterious hydrocarbon[1]. It contains an equal number of masked and unmasked carbons, suggesting that all π-electrons should be spin-paired (Fig. 1b). However, it cannot be represented by a Kekulé structure without leaving unpaired electrons. In its resonance structure, two unpaired electrons are always present. According to classic valence bond theory, it is challenging to reconcile how a diradical molecule can have all its π-electrons spin-paired.

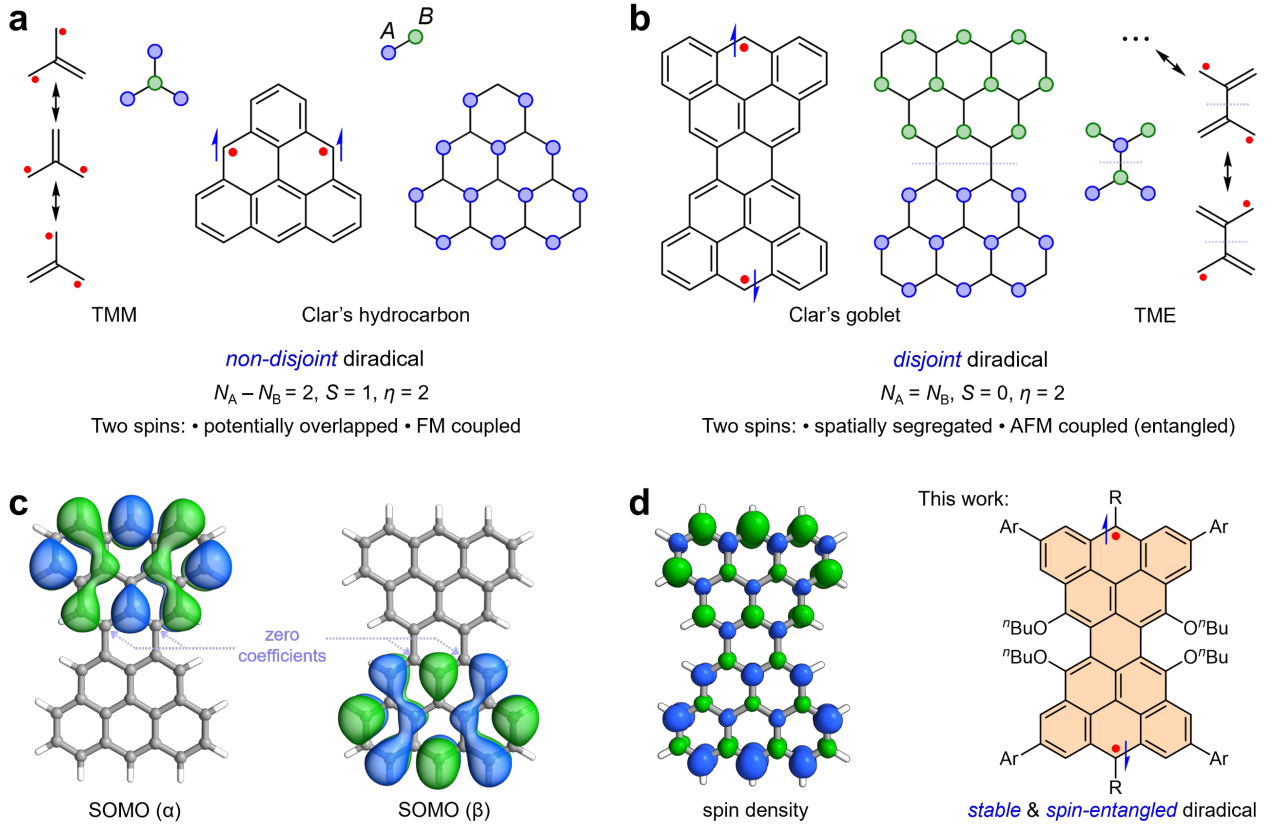

Fig. 1 | Illustration of the concept of spin-entanglement between the disjoint diradical in a graphene fragment – Clar's goblet, along with the achieved molecular design and properties in this work. a, **b**, Valence bond structures and bipartite lattice representations of non-disjoint diradical (**a**), and disjoint diradical (**b**). Blue and green circles represent A and B sublattice atoms, respectively. As for Clar's hydrocarbon and Clar's goblet, some sublattice atoms are not labeled for clarity, and all colored circles correspond to the maximum sets of non-adjacent sites. The total spin (S) is calculated by Lieb's theorem ($S = | N_A - N_B | / 2$). The nullity (η) is equal to the difference between the numbers of the maximum set of non-adjacent sites and the remaining sites. The dash lines in the disjoint diradical structures indicate that the two radicals can only be distributed on their respective halves in all resonance structures. **c**, **d**, DFT calculated SOMO (α), SOMO (β) (**c**), spin density distribution (**d**) of Clar's goblet at um06-2x/6-31g(d,p) level of theory. Herein, SOMOs are actually the same as NMBOs. R and Ar represent substituent groups.

Clar's goblet, with delocalized unpaired electrons in its π-conjugated sp^2-carbon skeleton, structurally belongs to the category of graphene fragment radicals[2-8]. These graphenic radicals possess distinct optical, electronic and magnetic properties, making them highly promising for applications in materials science[9-21]. Two terms, "disjoint" and "non-disjoint" have been used to

https://doi.org/10.26434/chemrxiv-2024-ks6xm **ORCID:** https://orcid.org/0000-0002-8231-0437 Content not peer-reviewed by ChemRxiv. **License:** CC BY 4.0

describe delocalized diradicals[22-23]. In non-disjoint diradicals, such as Clar's hydrocarbon (triangluene)[24-27] and trimethylenemethane (TMM)[28], two radicals can interchange positions through resonance structures (Fig. 1a). From the perspective of molecular orbital, two degenerate nonbonding molecular orbitals (NBMOs) spatially overlap, leading electrons to prefer unpaired spins to minimize repulsion, in accordance with Hund's rule[29]. This triplet ground state of non-disjoint diradicals can be readily determined by sublattice imbalance by using Lieb's theorem[30] or Ovchinnikov's rule[31]. On the contrary, in Clar's goblet or tetramethyleneethane (TME)[32], two degenerate NBMOs are disjoint (i.e., have no atoms in common. Fig. 1c). The two radicals are only distributed in separate halves, based on resonance structure analysis (Fig. 1b). Consequently, the two electrons have no spatial overlap and do not need to obey Hund's rule. Furthermore, they tend to have opposite spins, although the mechanism is still unclear and may involve dynamic spin polarization[33-35]. The calculated spin density distribution clearly illustrates the polarized distribution of the up and down spins in Clar's goblet (Fig. 1d). This unusual spin pairing between the two spatially separated electrons in Clar's goblet represents a form of spin entanglement[36,37]. Although this local spin entanglement is far from practical application, pursuing demonstration of this property remains crucial for understanding quantum phenomena at the molecular level.

Therefore, Clar's goblet has been a long-sought synthetic target for decades, motivating extensive advancements in synthetic chemistry[38-41], molecular structure and magnetism theory[42-45]. The primary challenge in the chemical synthesis of Clar's goblet is to find a feasible way to construct its topologically frustrated sp^2-C network with atomic precision, particularly the C–C bonds within the disjoint region. In addition, the high reactivity of radicals often leads to undesired decomposition. In 2020, Fasel and Feng's teams reported the on-surface synthesis of Clar's goblet and *in situ* investigation[39]. The properties obtained by on-surface chemistry are unavoidably influenced by the interactions with the gold surface. Moreover, many key properties of Clar's goblet are difficult to explore under the stringent conditions (e.g., on a metal surface, under ultrahigh vacuum) of on-surface chemistry, and thus are still hidden. Overall, the precise synthesis of Clar's goblet by wet chemistry and revealing its unusual physical properties remain a long-standing and highly important challenge. In this Article, we report on the solution-phase synthesis of Clar's goblet and deciphering its intriguing physical properties, especially the spin-entanglement between the two confined electrons. The key C–C bonds in the disjoint region are constructed by an intermolecular radical-radical coupling approach. Moreover, introducing bulky substituents at the periphery of Clar's goblet enhances its kinetical inertness, making it easier to handle during isolation and investigation. Temperature-dependent magnetic studies reveal an antiferromagnetic (AFM) coupling between the two spatially segregated spins in Clar's goblet, with an average spin-spin distance of 8.7 Å and coupling strength of –0.29 kcal/mol. This unique spin spatial segregation is further demonstrated by theoretical and experimental studies of the radical cation state of Clar's goblet. This work experimentally demonstrated what has been long expected theoretically: the two individual spins in the hydrocarbon – Clar's goblet are entangled in the ground state.

Results and discussion

Molecular design and synthesis of Clar's goblet

Based on retrosynthetic analysis, the skeleton of Clar's goblet can be viewed as the fusion of two

https://doi.org/10.26434/chemrxiv-2024-ks6xm **ORCID:** https://orcid.org/0000-0002-8231-0437 Content not peer-reviewed by ChemRxiv. **License:** CC BY 4.0

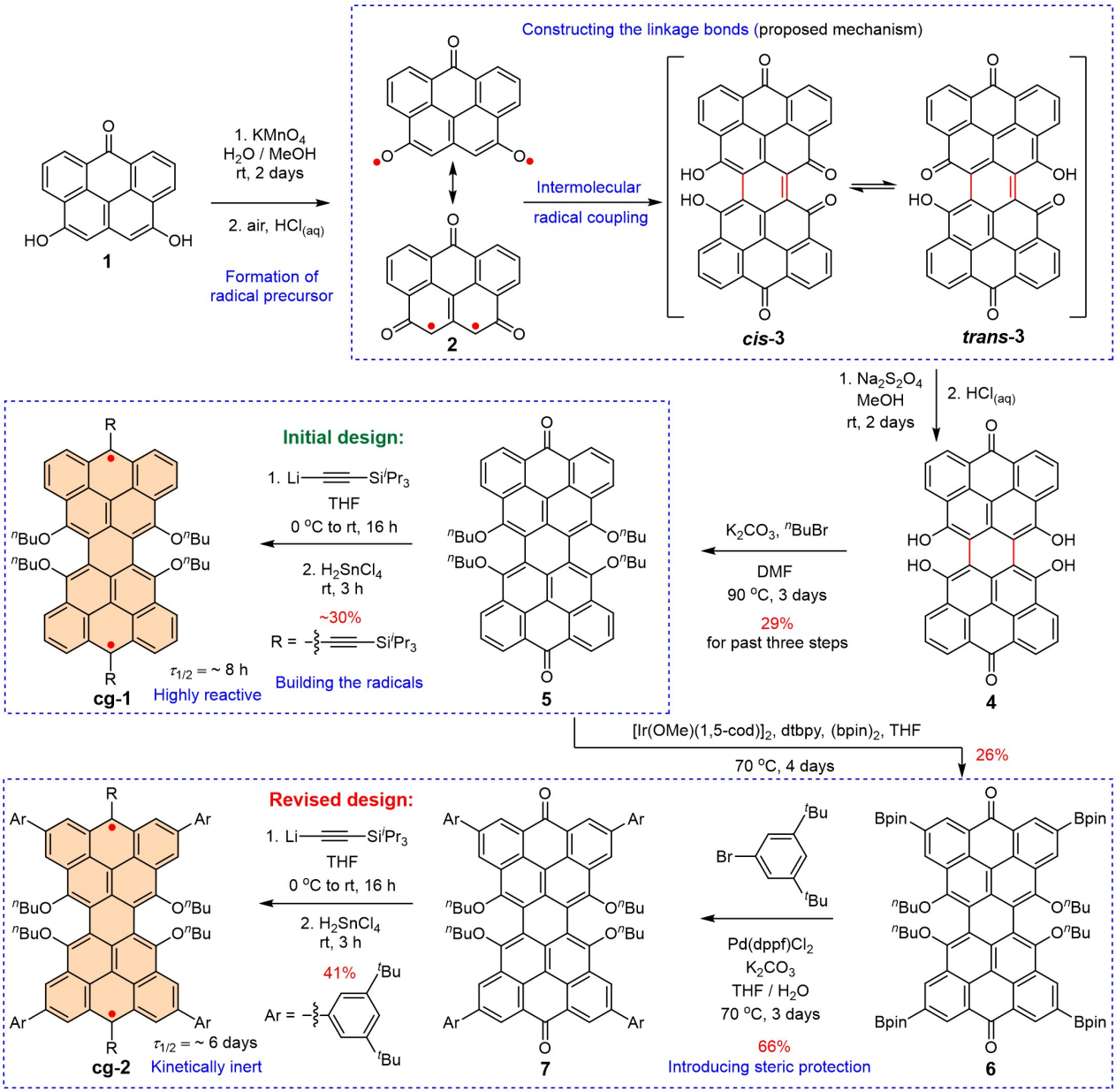

Fig. 2 | Molecular design and synthesis of the cg-1 and cg-2.

olympicenyl radicals[46], with two new C–C bonds formed in the disjoint region. Therefore, a straightforward synthetic strategy is to create these two connecting bonds between olympicenyl radicals or derivatives through intermolecular radical-radical coupling, which was also the idea behind Clar's attempt[1]. However, olympicenyl radicals or derivatives have zero spin density on these two bottom carbons, leading to the failure of radical-radical coupling. We thus designed a modified diradical precursor, making this strategy feasible (Fig. 2). Dihydroxyl naphthanthrone (**1**) was the starting compound, which was further transformed into diradical precursor **2** under the oxidative condition developed by Zeng's group[47,48]. The diradical precursor **2** has considerable spin density on the desired carbons, as suggested by its carbon-centered radical resonance structure. Intermolecular radical-radical coupling between two molecules of **2** and subsequent simultaneous dehydrogenation driven by aromaticity, led to the formation of the proposed intermediate **3**. This dimerized

https://doi.org/10.26434/chemrxiv-2024-ks6xm **ORCID:** https://orcid.org/0000-0002-8231-0437 Content not peer-reviewed by ChemRxiv. **License:** CC BY 4.0

intermediate **3** was further reduced into tetrahydroxyl **4** using $Na_2S_2O_4$. Due to their poor solubilities, intermediates **3** and **4** were directly used in the next steps without characterization. The hydroxyl groups in **4** were converted to *n*-butoxy (^{n}BuO) groups in **5** by reacting with excess K_2CO_3 and 1-bromobutane. The key precursor **5** with the target carbon skeleton can be fully characterized including single-crystal X-ray diffraction analysis (Supplementary Fig. 19). In the final step, treatment of diketone **5** with excess lithium (triisopropylsilyl)acetylide followed by reductive dehydroxylation with H_2SnCl_4 resulted in the formation of target Clar's goblet – **cg-1**. However, the high reactivity of **cg-1**, with an estimated half-life time ($\tau_{1/2}$) of 8 hours (Supplementary Fig. 18), limits further reliable characterization. We thus revised the molecular design of Clar's goblet to **cg-2** by introducing bulky aryl substituents at the periphery to increase its kinetical inertness. Ir-catalyzed borylation reaction of compound **5** produced compound **6** with four pinacol boronate (Bpin) groups. Subsequent Suzuki coupling reaction allowed us to install aryl substituents at the peripheral positions, yielding the diketone precursor **7**. This precursor underwent the same nucleophilic addition/reductive dehydroxylation steps to generate **cg-2**. The sterically hindered substituents successfully made **cg-2** more inert, with a substantially extended $\tau_{1/2}$ of 6 days (Supplementary Fig. 18), allowing for in-depth investigation.

X-ray crystallographic analysis

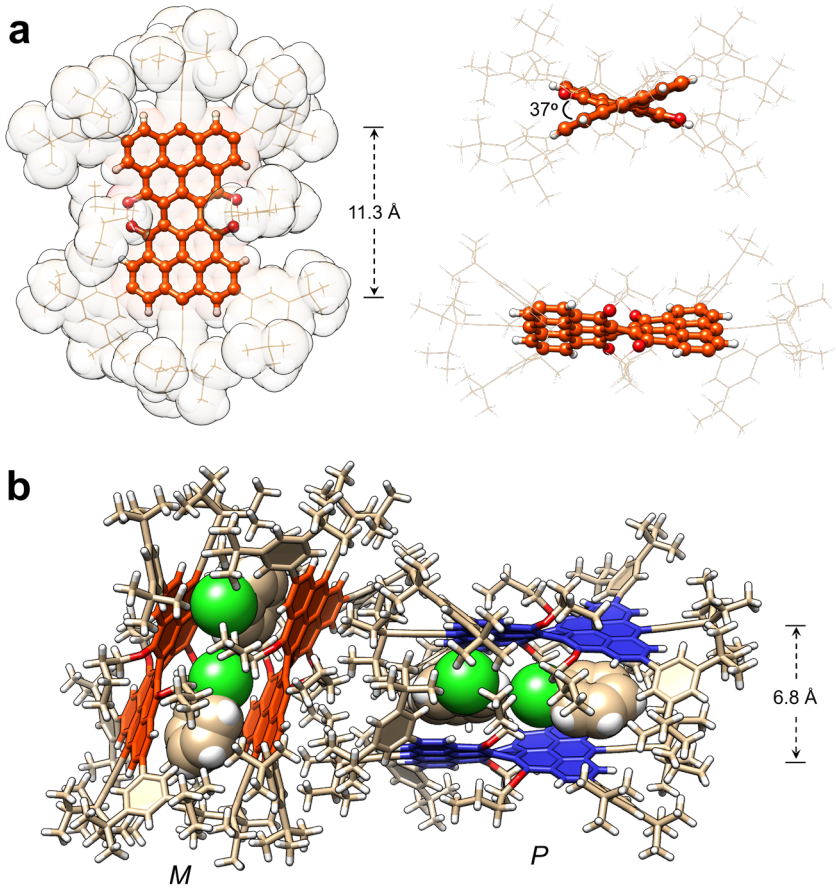

Fig. 3 | Single crystal structure and super-structure of cg-2. a, Different views of a single **cg-2**. **b**, Super-structure of **cg-2**, showing the racemic composition and packing of *M*- and *P*- enantiomers. Two solvent molecules (chlorobenzene) are encapsulated between two same enantiomers of **cg-2**, driven by intermolecular interactions including hydrogen bonding, π•••π interaction, and CH•••π interaction.

https://doi.org/10.26434/chemrxiv-2024-ks6xm **ORCID:** https://orcid.org/0000-0002-8231-0437 Content not peer-reviewed by ChemRxiv. **License:** CC BY 4.0

Single crystals of **cg-2** were obtained by slow vapor diffusion of acetonitrile into its chlorobenzene solution in a glovebox filled with nitrogen gas. Crystallographic analysis unambiguously demonstrated the structure. The skeleton of Clar's goblet is surrounded by peripheral bulky substituents, with a head-to-tail distance of 11.3 Å (Fig. 3a). The presence of middle ^{n}BuO chains induces a twist in the backbone with an angle of about 37°. Moreover, this twisted backbone imparts intrinsic chirality to **cg-2**, resulting in *P*- and *M*- enantiomers. The packing structure shows the racemic composition (Fig. 3b). Interestingly, two identical enantiomers form a pseudo-molecular box, encapsulating two chlorobenzene molecules inside. The formation of this super-structure is driven by hydrogen bonding, π•••π interactions, and CH•••π interactions (Supplementary Fig. 21). The distance between the top and bottom **cg-2** in the super-structure is approximately 6.8 Å, indicating weak intermolecular spin-spin interactions.

cw-EPR Studies probing the intramolecular spin-spin interaction

As explained in the introduction, the two electrons in Clar's goblet are spatially segregated and cannot be paired by forming a chemical bond. The long-standing question is: how do these two individual electrons interact with each other? In principle, a two-spin system can exist in a magnetically active triplet state when the spins are aligned, or in a magnetically silent singlet state when the spins are opposite. Alternatively, if spin-spin interaction is very weak, the system might behave like an almost independent doublet state. Thus, the key to addressing this question is to distinguish the spin ground state of Clar's goblet. Continuous-wave electron paramagnetic resonance (cw-EPR) measurement was first used to probe the interaction between the two spins. At 170 K, the spectrum of **cg-2** in the frozen toluene-d_8 solution shows resonance signals composed of two components: zero-field splitting (ZFS) from a triplet (S = 1) component and central peaks from a doublet (S = 1/2) component, which can be readily separated by simulation (Fig. 4c, simulation parameters are attached in the Supplementary Information). A forbidden transition ($|\Delta m_s| = 2$) signal is also observed (m_s refers to magnetic quantum number). The characteristic ZFS and half-field absorption provide solid evidence[49] for the existence of triplet state in Clar's goblet and rule out the possibility that the two spins are weakly interacted. Furthermore, ZFS parameters of $|D|$ = 114.5 MHz and $|E|$ = 15.7 MHz are obtained from simulations. Using the equation $D = 1.39 \times 10^4 (g/r^3)$ where unpaired electrons are considered as point-dipoles[50], the average spin-spin distance in **cg-2** is determined as 8.7 Å, further supporting the spatial segregation of the two spins (Fig. 4d). Additionally, the doublet component in cw-EPR spectrum is proposed to be monoradical impurities with structures similar to **cg-2**. The observation of doublet signals in the EPR measurement of diradicals is very common, and the origin of the monoradical impurities includes the interactions or reactions with oxygen, solvents, light or intermolecular interactions[51].

Pulse-EPR and SQUID studies revealing the singlet ground state

To further identify the spin ground state of Clar's goblet, pulse-EPR was used because of its high signal reliability at low temperatures. The echo-detected field-swept (EDFS) spectra of **cg-2** were recorded at 10 K, 50 K, and 100 K, respectively. These EDFS spectra can be accurately deconvoluted into one doublet and one triplet component with relative weights by simulations (Fig. 4a, simulation parameters are attached in the Supplementary Information). As the temperature increases from 10 K to 100 K, the triplet component substantially increases from 0.36 to 1.70 relative to the doublet component (its weight sets to 1). This thermal populated property clearly demonstrates that the

https://doi.org/10.26434/chemrxiv-2024-ks6xm **ORCID:** https://orcid.org/0000-0002-8231-0437 Content not peer-reviewed by ChemRxiv. **License:** CC BY 4.0

triplet state is the excited state of **cg-2**. To further verify the spin states of the proposed doublet and triplet components in the EDFS spectra, echo-detected nutation experiments were performed using the pulse sequency t_p-*T*-π/2-τ-π-τ-echo (*T* refers to waiting time). In nutation experiments, a microwave nutation pulse with duration t_p, is applied to drive the spin system in the sample into a superposition of its two m_s levels of a given resonance. With increasing nutation pulse length, the spin system is cycled through all arbitrary superpositions of the two m_s levels, resulting in the Rabi oscillations in the detected signal. As shown in Fig. 4b, the Rabi oscillations were recorded at the magnetic field of 3401 G, temperature of 10 K and 100 K, respectively. After fast Fourier transformation, the oscillation data are transformed into two separate frequencies corresponding to the doublet and triplet specie. The spin states of these two species are confirmed because the ratio of the Rabi frequency for the assigned triplet species ($\Omega^{m_{\pm1}\leftrightarrow m_0}$) to that of the doublet species ($\Omega^{m_{-1/2}\leftrightarrow m_{+1/2}}$) is very close to the theoretical value of $\sqrt{2}$ (Eq 1 in the Supplementary Information, and Supplementary Fig. 25). In addition, the intensity of the triplet species relative to the doublet species noticeably increases at 100 K compared to at 10 K (Fig. 4b inset). This observation further demonstrates that the triplet state is the thermally populated excited state of **cg-2**.

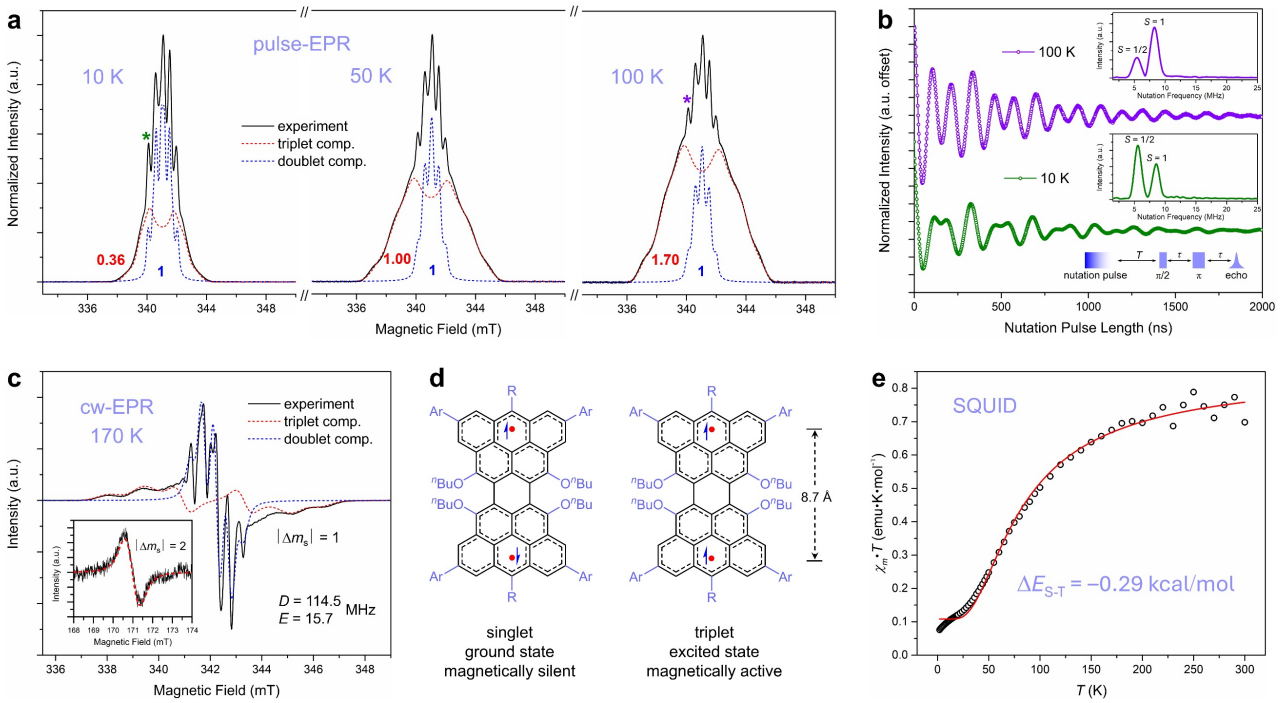

Fig. 4 | Deciphering the spin ground state of cg-2 and the dipolar interaction between the two radicals. **a**, Experimental and simulated Echo-detected field-swept (EDFS) spectra of **cg-2** in frozen deuterated toluene solution. The red and blue numbers correspond to the simulated weights of the triplet component and the doublet component. **b**, Rabi oscillations of **cg-2** at 10 K and 100 K, respectively. Data were collected at 3401 G and 6 dB attenuation of power of microwave pulse. The positions of magnetic field 3401 G in the spectra at 10 K and 100 K are labelled with green and purple stars, respectively. Inset: Nutation frequency diagrams generated by Fourier transformation. **c**, Experimental and simulated cw-EPR spectrum of **cg-2** in frozen deuterated toluene solution. All simulation parameters are included in the Supplementary Information. **d**, Schematic illustration of the spin ground state and excited state of **cg-2**. **e**, SQUID measurement and fitting curve of **cg-2** in powder form.

https://doi.org/10.26434/chemrxiv-2024-ks6xm **ORCID:** https://orcid.org/0000-0002-8231-0437 Content not peer-reviewed by ChemRxiv. **License:** CC BY 4.0

Next, superconducting quantum interference device (SQUID) measurement was performed on freshly prepared crystalline powder of **cg-2** to quantify the energy gap ($\Delta E_{S\text{-}T}$) between the singlet ground state and the triplet excited state, more fundamentally, the coupling strength between the two spins in **cg-2**. The product value of the molar magnetic susceptibility and temperature (χ_m•T) rapidly increase from 25 K, and gradually approaches saturation after 200 K (Fig. 4e). This is the characteristic feature of thermally populated transition from the magnetically silent singlet state to the magnetically active triplet state. By fitting the χ_m•T -T curve with Bleaney-Bowers equation[52] (Eq 3 in the Supplementary Information, the contribution from doublet impurities is treated as a constant in the fitting), $\Delta E_{S\text{-}T}$ was determined to be –0.29 kcal/mol, which is consistent with DFT-calculated value –0.35 kcal/mol. This $\Delta E_{S\text{-}T}$ value is considerably smaller than the energy gaps for many open-shell singlet diradicaloid systems[53-56], suggesting the coupling strength between the spatially segregated spins in **cg-2** is much weaker than bonding interaction. In addition, χ_m•T value rapidly decreases below 25 K, indicating that the influence of intermolecular AFM coupling can no longer be ignored at extremely low temperatures. At present, the interaction between the two spatially segregated electrons in **cg-2** has been clearly revealed: the two electrons can feel the existence of each other and keep their spins paired in the ground state, suggesting a spin entanglement in Clar's goblet. The singlet ground state can be thermally excited to triplet state. Theoretically calculated spin density distribution (Supplementary Fig. 23) of the singlet state of **cg-2** retains the same spin polarization feature as the pristine Clar's goblet, with the up and down spins separately localized on the two halves.

Spin dynamics studies

Another important property of **cg-2** is its ability to maintain spin state, which is crucial for exploring spin-based applications[57,58]. In radical systems, spin relaxation from excited state to ground state is mainly triggered by the interactions with surrounding environment or itself, as the rate of spontaneous relaxation is negligible. Thereby, the spin-lattice relaxation time (T_1) and coherence time (T_m) of **cg-2** were measured to be 96 μs and 0.8 μs at 100 K and the field of 3401 G (Supplementary Fig. 26), respectively, using inversion-recovery method (π-T-π/2-τ-π-τ-echo) and modified Hahn-echo pulse sequency (π/2-τ-π-τ-echo). The relatively shorter relaxation time of **cg-2**, compared with typical carbon-centered radicals[16,59,60], are probably due to the influence of numerous magnetic proton nuclei on the substituents. Moreover, the Rabi frequency $\Omega^{m_{\pm1}\leftrightarrow m_0}$ of 8.21 MHz for **cg-2** provides the experimental timescale ($\tau_{spin\text{-}flip}$ = 61 ns) for one spin-flip operation ($\Omega = \left(2\tau_{\mathrm{spin-flip}}\right)^{-1}$), suggesting that the relaxation time of **cg-2** is sufficiently long for multiple spin-flip operations. This is a requisite condition for performing molecular spin-based quantum computation.

Electrochemical and optical properties

Cyclic voltammetry (CV) and differential pulse voltammetry (DPV) measurements of **cg-2** in dry CH_2Cl_2 revealed two successive redox waves, Ⅰ and Ⅱ with the half-wave potentials $E_{1/2}$ at –0.21 V and 0 V (all values vs Fc/Fc^+), respectively (Fig. 5a). The redox waves Ⅰ and Ⅱ correspond to stepwise one-electron oxidations of **cg-2** from its neutral diradical state to the radical cation state, then the dication state. These oxidation states were obtained by chemical oxidation with $NO{\cdot}SbF_6$ and characterized by UV-vis-NIR absorption spectroscopy (Fig. 5b). The neutral diradical state of **cg-2**

https://doi.org/10.26434/chemrxiv-2024-ks6xm **ORCID:** https://orcid.org/0000-0002-8231-0437 Content not peer-reviewed by ChemRxiv. **License:** CC BY 4.0

shows weak absorption bands at 675 nm and longer wavelengths region. According to time-dependent DFT calculation, these weak absorption bands could be assigned to the forbidden transitions from SOMO-α to LUMO-α and SOMO-β to LUMO-β (Supplementary Fig. 24). The radical cation and dication states of **cg-2** exhibit similar absorption features: an intense band at 669 nm and a broad band centered at 1022 and 924 nm, respectively, indicating the structural similarity in their molecular orbitals related to electronic transitions (Supplementary Fig. 24).

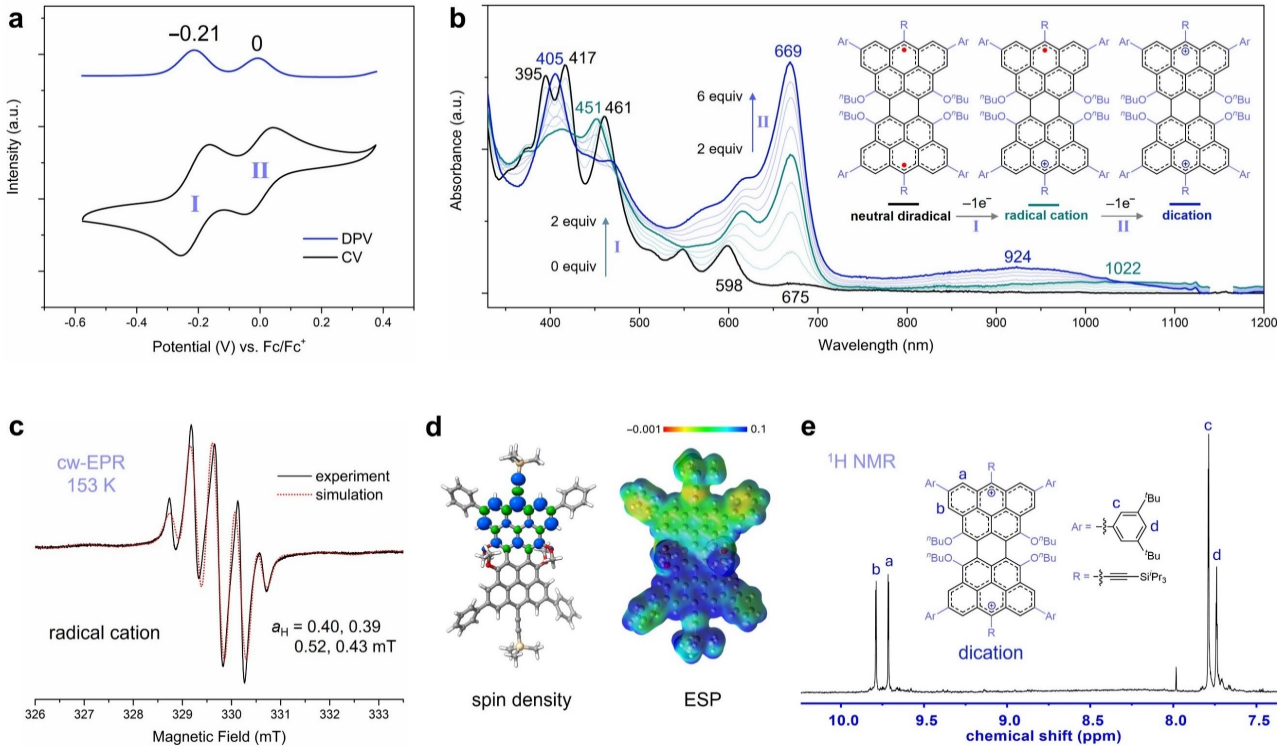

Fig. 5 | Redox behavior of cg-2, and characterization of its different oxidation states, revealing the spin/charge spatial segregation property. a, CV and DPV (in 0.1 M $^{n}Bu_4N{\cdot}PF_6/CH_2Cl_2$, scan rate: 50 mV•s^{-1} for CV, step length: 10 mV for DPV, rt) of **cg-2**. **b**, UV-vis-NIR absorption spectra (in CH_2Cl_2) of **cg-2** and its oxidized species. The oxidized species were obtained by chemical oxidation titration with $NO{\cdot}SbF_6$. **c**, Experimental and simulated cw-EPR spectrum of the radical cation state of **cg-2** in frozen CH_2Cl_2 solution. **d**, DFT calculated spin density distribution and electrostatic potential surface (ESP) of the radical cation state of **cg-2** at m06-2x/6-311g(d,p) level of theory. The value of electrostatic potential is in arbitrary units. **e**, ^{1}H NMR spectrum (500 MHz, CD_2Cl_2, rt) of the dication state of **cg-2**.

Spatially segregated spin and charge in the radical cation state

Similar to the neutral diradical state, the electron and charge in the radical cation state of **cg-2** are also spatially segregated (i.e., the electron is distributed on one half, and the positive charge is distributed on the other half). This unique electronic property of the radical cation state of **cg-2** is also predicted by DFT calculated spin density distribution and electrostatic potential surface (Fig. 5d). cw-EPR spectrum of the radical cation state of **cg-2** was measured in frozen CH_2Cl_2 at 153 K to suppress the rapid tumbling motion in solution. The signal is split into a quintet by four anisotropic protons with simulated hyperfine coupling constants of a_H = 0.40, 0.39, 0.43 and 0.52 mT (Fig. 5c). This observation provides direct experimental evidence for the spatially segregated spin in the

https://doi.org/10.26434/chemrxiv-2024-ks6xm **ORCID:** https://orcid.org/0000-0002-8231-0437 Content not peer-reviewed by ChemRxiv. **License:** CC BY 4.0

radical cation state of **cg-2**, because if the spin is globally delocalized over the whole molecule, the EPR signal will be split into a nonet by eight anisotropic protons, each with the halved a_H. It should be noted that as the temperature increases, a nonet EPR signal appears, probably due to the averaging effect caused by tumbling motion or by thermally populated electron hoping from one half to the other half (Supplementary Fig. 27). The dication state of **cg-2** recovers its closed-shell electronic structure, therefore the ^{1}H NMR measurement was performed. The protons H_a and H_b appear at downfield region (Fig. 5e), indicating the deshielding effect brought by the presence of positive charge.

Conclusion

In summary, we realized the solution-phase synthesis and isolation of the Clar's goblet derivative **cg-2** with bulky substituents. The precise construction of its topologically frustrated sp^2-C network was achieved through an intermolecular radical-radical coupling approach. The synthetic scalability and kinetical inertness of **cg-2** allow us to experimentally elucidate the long-standing doubt about the interaction between the two spins in Clar's goblet. Magnetic studies reveal that the two spins are spatially segregated in Clar's goblet with an average distance of 8.7 Å, and are AFM coupled in the ground state. The singlet ground state can be thermally excited to a triplet state with an $\Delta E_{S\text{-}T}$ of –0.29 kcal/mol. Furthermore, the spatial segregation of spin/charge can be directly observed through EPR splitting in the radical cation state of **cg-2**. This spin pairing discovered in Clar's goblet not only suggests a spin entanglement phenomenon at the molecular scale, but also may enable practical logic operations in spin-based quantum computation. Finally, we hope this study could inspire and motivate further efforts to uncover the fundamental mechanism of this spin entanglement and push the application of tailor-made molecular spins in quantum information technologies.

Data availability

The data that support the findings of this study are available in the Supplementary Information. Crystallographic data for the structures reported in this Article have been deposited at the Cambridge Crystallographic Data Centre, under deposition numbers CCDC 2376440 (**5**) and 2376442 (**cg-2**). Copies of the data can be obtained free of charge via https://www.ccdc.cam.ac.uk/structures/. Source data are provided with this paper.

Acknowledgements

J.W. acknowledges the financial support from Singapore MOE Tier 2 projects (MOE-T2EP10222-0003 and MOE-T2EP10221-0005) and A*STAR MTC IRG grant (M22K2c0083). S.-D.J. thanks the Natural Science Foundation of China (22325503, 22250001, U20A6002).

Author contributions

T.J. and J.W. conceived the project, designed the research, and prepared the manuscript. T.J. carried out most of experiments and analyzed the data. J.W. supervised the project. C.-H.W. and Y.-S.Z. contributed to the pulse-EPR measurements. X.M. and S.W. contributed to the X-ray crystallographic analyses. S.-D.J. supervised the EPR and magnetic studies. All authors discussed and commented on

https://doi.org/10.26434/chemrxiv-2024-ks6xm **ORCID:** https://orcid.org/0000-0002-8231-0437 Content not peer-reviewed by ChemRxiv. **License:** CC BY 4.0

the manuscript.

Competing interests

The authors declare no competing interests.

References

1. Clar, E., & Mackay, C. C. Circobiphenyl and the attempted synthesis of 1: 14, 3: 4, 7: 8, 10: 11-tetrabenzoperopyrene. *Tetrahedron* **28**, 6041-6047 (1972).
2. Morita, Y., Suzuki, S., Sato, K. & Takui, T. Synthetic organic spin chemistry for structurally well-defined open-shell graphene fragments. *Nat. Chem.* **3**, 197-204 (2011).
3. Zeng, W. & Wu, J. Open-shell graphene fragments. *Chem* **7**, 358-386 (2021).
4. Kubo, T. Syntheses and properties of open-shell π-conjugated molecules. *Bull. Chem. Soc. Jpn*. **94**, 2235−2244 (2021).
5. Xiang, Q. & Sun, Z. Doublet open-shell graphene fragments. *Chem. Asian J.* **17**, e202200251 (2022).
6. Ahmed, J., & Mandal, S. K. Phenalenyl radical: Smallest polycyclic odd alternant hydrocarbon present in the graphene sheet. *Chem. Rev*. **122**, 11369-11431 (2022).
7. Yokoi, H., Hiroto, S., & Shinokubo, H. Reversible σ-bond formation in bowl-shaped π-radical cations: the effects of curved and planar structures. *J. Am. Chem. Soc.* **140**, 4649-4655 (2018).
8. Jiao, T. et al. Synthesis of monolayer and persistent bilayer graphene fragments by using a radical-mediated coupling approach. *Nat. Synth.* **2**, 1104-1115 (2023).
9. Pal, S. K. et al. Resonating valence-bond ground state in a phenalenyl-based neutral radical conductor. *Science* **309**, 281-284 (2005).
10. Kubo, T. et al. Synthesis, intermolecular interaction, and semiconductive behavior of a delocalized singlet biradical hydrocarbon. *Angew. Chem. Int. Ed.* **44**, 6564-6568 (2005).
11. Pariyar, A. et al. Switching closed-shell to open-shell phenalenyl: toward designing electroactive materials. *J. Am. Chem. Soc.* **137**, 5955-5960 (2015).
12. Rudebusch, G. E. et al. Diindeno-fusion of an anthracene as a design strategy for stable organic biradicals. *Nat. Chem*. **8**, 753–759 (2016).
13. Mukherjee, A., Sau, S. C., & Mandal, S. K. Exploring closed-shell cationic phenalenyl: From catalysis to spin electronics. *Acc. Chem. Res.* **50**, 1679-1691 (2017).
14. Kushida, T. et al. Boron-stabilized planar neutral π-radicals with well-balanced ambipolar charge-transport properties. *J. Am. Chem. Soc.* **139**, 14336-14339 (2017).
15. Ravat, P., Šolomek, T., Häussinger, D., Blacque, O. & Juríček, M. Dimethylcethrene: A chiroptical diradicaloid photoswitch. *J. Am. Chem. Soc.* **140**, 10839-10847 (2018).
16. Lombardi, F. et al. Quantum units from the topological engineering of molecular graphenoids. *Science* **366**, 1107-1110 (2019).
17. Jousselin-Oba, T. et al. Excellent semiconductors based on tetracenotetracene and pentacenopentacene: From stable closed-shell to singlet open-shell. *J. Am. Chem. Soc.* **141**, 9373-9381 (2019).
18. Imran, M., Wehrmann, C. M., & Chen, M. S. Open-shell effects on optoelectronic properties: Antiambipolar charge transport and anti-kasha doublet emission from a N-substituted bisphenalenyl. *J. Am. Chem. Soc.* **142**, 38-43 (2019).
19. Zong, C. et al. Isomeric dibenzoheptazethrenes for air-stable organic field-effect transistors. *Angew. Chem. Int. Ed.* **60**, 16230-16236 (2021).
20. Prajapati, B. et al. Tetrafluorenofulvalene as a sterically frustrated open-shell alkene. *Nat. Chem.* **15**, 1541-1548

https://doi.org/10.26434/chemrxiv-2024-ks6xm **ORCID:** https://orcid.org/0000-0002-8231-0437 Content not peer-reviewed by ChemRxiv. **License:** CC BY 4.0

(2023).
21. Wang, W. et al. A triply negatively charged nanographene bilayer with spin frustration. *Angew. Chem. Int. Ed.* **62**, e202217788 (2023).
22. Borden, W. T., & Davidson, E. R. Effects of electron repulsion in conjugated hydrocarbon diradicals. *J. Am. Chem. Soc.* **99**, 4587-4594 (1977).
23. Lineberger, W. C., & Borden, W. T. The synergy between qualitative theory, quantitative calculations, and direct experiments in understanding, calculating, and measuring the energy differences between the lowest singlet and triplet states of organic diradicals. *Phys. Chem. Chem. Phys.* **13**, 11792-11813 (2011).
24. Inoue, J. *et al.* The first detection of a Clar's hydrocarbon, 2,6,10-tri-*tert*-butyltriangulene: A ground-state triplet of non-Kekulé polynuclear benzenoid hydrocarbon. *J. Am. Chem. Soc.* **123**, 12702-12703 (2001).
25. Pavliček, N. et al. Synthesis and characterization of triangulene. *Nat. Nanotechnol*. **12**, 308–311 (2017).
26. Arikawa, S., Shimizu, A., Shiomi, D., Sato, K. & Shintani, R. Synthesis and isolation of a kinetically stabilized crystalline triangulene. *J. Am. Chem. Soc.* **143**, 19599-19605 (2021).
27. Valenta, L. et al. Trimesityltriangulene: a persistent derivative of Clar's hydrocarbon. *Chem. Commun.* **58**, 3019-3022 (2022).
28. Dowd, P. Trimethylenemethane. *Acc. Chem. Res.* **5**, 242-248 (1972).
29. Hund, F. Zur deutung verwickelter spektren, insbesondere der elemente scandium bis nickel. *Z. Phys.* **33**, 345-371 (1925).
30. Lieb, E. H. Two theorems on the Hubbard model. *Phys. Rev. Lett*. **62**, 1201–1204 (1989).
31. Ovchinnikov, A. A. Multiplicity of the ground state of large alternant organic molecules with conjugated bonds: (Do Organic Ferromagnetics Exist?). *Theor. Chim. Acta* **47**, 297-304 (1978).
32. Dowd, P. Tetramethyleneethane. *J. Am. Chem. Soc.* **92**, 1066-1068 (1970).
33. Kollmar, H., & Staemmler, V. Violation of Hund's rule by spin polarization in molecules. *Theor. Chim. Acta* **48**, 223-239 (1978).
34. Salem, L. The sudden polarization effect and its possible role in vision. *Acc. Chem. Res.* **12**, 87-92 (1979).
35. Karafiloglou, P. The double (or dynamic) spin polarization in π diradicals. *J. Chem. Educ.* **66**, 816-817 (1989).
36. Burkard, G. Spin-entangled electrons in solid-state systems. *J. Phys.: Condens. Matter* **19**, 233202 (2007).
37. Troiani, F., & Affronte, M. Molecular spins for quantum information technologies. *Chem. Soc. Rev.* **40**, 3119-3129 (2011).
38. Liu, J., & Feng, X. Synthetic Tailoring of graphene nanostructures with zigzag-edged topologies: progress and perspectives. *Angew. Chem. Int. Ed.* **59**, 23386-23401 (2020).
39. Mishra, S. et al. Topological frustration induces unconventional magnetism in a nanographene. *Nat. Nanotechnol.* **15**, 22-28 (2020).
40. Zhao, C. et al. Tailoring magnetism of graphene nanoflakes via tip-controlled dehydrogenation. *Phys. Rev. Lett.* **132**, 046201 (2024).
41. Zhao, C. et al. Tunable topological phases in nanographene-based spin-1/2 alternating-exchange Heisenberg chains. *arXiv* 2024, *doi: 10.48550/arXiv.2402.13590.*
42. Pogodin, S., & Agranat, I. Clar goblet and related non-Kekulé benzenoid LPAHs. A theoretical study. *J. Org. Chem.* **68**, 2720-2727 (2003).
43. Wang, W. L., Yazyev, O. V., Meng, S., & Kaxiras, E. Topological frustration in graphene nanoflakes: magnetic order and spin logic devices. *Phys. Rev. Lett.* **102**, 157201 (2009).
44. Ortiz, R. et al. Exchange rules for diradical π-conjugated hydrocarbons. *Nano Lett.* **19**, 5991-5997 (2019).
45. Gil-Guerrero, S., Melle-Franco, M., Peña-Gallego, Á., & Mandado, M. Clar goblet and aromaticity driven multiradical nanographenes. *Chem. Eur. J.* **26**, 16138-16143 (2020).

https://doi.org/10.26434/chemrxiv-2024-ks6xm **ORCID:** https://orcid.org/0000-0002-8231-0437 Content not peer-reviewed by ChemRxiv. **License:** CC BY 4.0

46. Xiang, Q. *et al.* Stable olympicenyl radicals and their π-dimers. *J. Am. Chem. Soc.* **142**, 11022-11031 (2020).
47. Wei, H. et al. A facile approach toward 1, 2-diazabenzo [*ghi*] perylene derivatives: structures and electronic properties. *Chem. Commun.* **53**, 6740-6743 (2017).
48. Li, Y. et al. *Bay*-and *ortho*-octasubstituted perylenes. *Org. Lett.* **19**, 5094-5097 (2017).
49. Abe, M. Diradicals. *Chem. Rev.* **113**, 7011-7088 (2013).
50. Eaton, S. S., More, K. M., Sawant, B. M., & Eaton, G. R. Use of the ESR half-field transition to determine the interspin distance and the orientation of the interspin vector in systems with two unpaired electrons. *J. Am. Chem. Soc.* **105**, 6560-6567 (1983).
51. Moise, G. et al. The electronic spin state of diradicals obtained from the nuclear perspective: the strange case of Chichibabin radicals. *ChemRxiv.* 2024, doi:10.26434/chemrxiv-2024-mktsd.
52. Bleaney, B. & Bowers, K. D. Anomalous paramagnetism of copper acetate. *Proc. R. Soc. Lond. Ser. A* **214**, 451–465 (1952).
53. Kubo, T. Recent progress in quinoidal winglet biradical molecules. *Chem. Lett.* **44**, 111-122 (2014).
54. Zeng, Z. et al. Pro-aromatic and anti-aromatic π-conjugated molecules: an irresistible wish to be diradicals. *Chem. Soc. Rev.* **44**, 6578-6596 (2015).
55. Y. Gopalakrishna, T., Zeng, W., Lu, X. & Wu, J. From open-shell singlet diradicaloids to polyradicaloids. *Chem. Commun.* **54**, 2186-2199 (2018).
56. Wu, J. *Diradicaloids*. (Jenny Stanford Publishing, 2022).
57. Sanvito, S. Molecular spintronics. *Chem. Soc. Rev.* **40**, 3336-3355 (2011).
58. Gaita-Ariño, A., Luis, F., Hill, S., & Coronado, E. Molecular spins for quantum computation. *Nat. Chem.* **11**, 301-309 (2019).
59. Lombardi, F. et al. Synthetic tuning of the quantum properties of open-shell radicaloids. *Chem* **7**, 1363-1378 (2021).
60. Zhang, D. et al. An air-stable carbon-centered triradical with a well-addressable quartet ground State. *J. Am. Chem. Soc.* **146**, 21752-21761 (2024).

https://doi.org/10.26434/chemrxiv-2024-ks6xm **ORCID:** https://orcid.org/0000-0002-8231-0437 Content not peer-reviewed by ChemRxiv. **License:** CC BY 4.0